Published in final edited form as:
J Comp Neurol. 2014 February 15; 522(3): . doi:10.1002/cne.23440.

The Subcellular Localization of Intercellular Adhesion Molecule-5 (Telencephalin) in the Visual Cortex is not Developmentally Regulated in the Absence of Matrix Metalloproteinase-9

Emily A. Kelly[1], **Marie-Eve Tremblay**[1,*], **Carl G. Gahmberg**[2], **Li Tian**[3,†], and **Ania K. Majewska**[1,†]

[1]Neurobiol & Anat., Univ. Rochester, NY [2]Dept. of Biosci, Univ. of Helsinki, Helsinki, Finland
[3]Neurosci. Ctr., Univ. of Helsinki, Helsinki, Finland

Abstract

The telencephalon-associated intercellular adhesion molecule 5 (Telencephalin; ICAM-5) regulates dendritic morphology in the developing brain. *In vitro* studies have shown that ICAM-5 is predominantly found within dendrites and immature dendritic protrusions, with reduced expression in mushroom spines, suggesting that ICAM-5 downregulation is critical for the maturation of synaptic structures. However, developmental expression of ICAM-5 has not been explored in depth at the ultrastructural level in intact brain tissue. To investigate the ultrastructural localization of ICAM-5 with transmission electron microscopy, we performed immunoperoxidase histochemistry for ICAM-5 in mouse visual cortex at postnatal day (P)14, a period of intense synaptogenesis, and at P28, when synapses mature. We observed the expected ICAM-5 expression in dendritic protrusions and shafts at both P14 and P28. ICAM-5 expression in these dendritic protrusions decreased in prevalence with developmental age to become predominantly localized to dendritic shafts by P28. To further understand the relationship between ICAM-5 and the endopeptidase metalloproteinase-9 (MMP-9), which mediates ICAM-5 cleavage following glutamate activation during postnatal development, we also explored ICAM-5 expression in MMP-9 null animals. This analysis revealed a similar expression of ICAM-5 in dendritic elements at P14 and P28; however an increased prevalence of ICAM-5 was noted in dendritic protrusions at P28 in the MMP-9 null animals, indicating that in the absence of MMP-9, there is no developmental shift in ICAM-5 subcellular localization. Our ultrastructural observations shed light on possible functions mediated by ICAM-5 and their regulation by extracellular proteases.

Corresponding Authors: Ania K. Majewska, University of Rochester, School of Medicine and Dentistry, Department of Neurobiology and Anatomy, Center for Visual Science, 601 Elmwood Avenue, Box 603, Rochester, New York 14642, Ania_Majewska@urmc.rochester.edu. Li Tian, Neuroscience Center, University of Helsinki, Viikinkaari 4, PO Box 56, Fin-00014, Helsinki, Finland, li.tian@helsinki.fi.
†authors contributed equally
*Present address: Dept. of Molecular Medicine, Université Laval, Québec

Conflict of Interest Statement
The authors have no conflict of interests to report.

Roles of Authors
All authors had full access to the contents of this manuscript and take responsibility for the veracity of the findings and presentation of data. Experiment design: E.A.K., A.K.M.; Acquisition of data: E.A.K.; Statistical analysis: E.A.K.; Manuscript preparation and draft: E.A.K.; Critical revision of the manuscript and intellection contribution: E.A.K., M.E.T., L.T., C.G., A.K.M.; Technical and material contribution: M.E.T, L.T., C.G.

Keywords

ICAM-5; dendrite; electron microscopy; plasticity; telencephalin; MMP-9

Introduction

The intercellular adhesion molecules (ICAMs) form a major subgroup within the immunoglobulin superfamily (IgSF), functioning primarily to mediate leukocyte adhesion through binding to the leukocyte-specific β_2 integrins (lymphocyte function associated antigen 1 (LFA-1); CD11/CD18) (Larson and Springer, 1990; Gahmberg, 1997; Gahmberg et al., 1997; Gahmberg et al., 2008; Zhang et al., 2008). As a member of this family, ICAM-5 (Telencephalin, TLCN) contains nine Ig-like domains that most closely resemble those of ICAMs that function in cell-cell interactions. Interestingly, ICAM-5 is the first example of a dendrite-specific cell adhesion molecule (Yoshihara and Mori, 1994; Yoshihara et al., 1994) restricting its expression to the soma-dendritic membrane of subsets of telencephalic neurons, but not to the axonal membrane (as shown in mouse, rat and rabbit) (Benson et al., 1998; Mitsui et al., 2005). Given this expression pattern, ICAM-5 has been postulated to regulate dendritic morphology and function.

The onset of ICAM-5 expression at birth parallels the timing of dendritic development and synapse formation in the telencephalon (Mori et al., 1987; Oka et al., 1990; Yoshihara et al., 1994). ICAM-5 is concentrated in dendritic shafts, dendritic filopodia, and thin immature spines *in vitro* (Matsuno et al., 2006), and has recently been observed at the sites of synaptic contacts (Ning et al., 2013). Convincing evidence suggests that ICAM-5 is an important regulator of spine maturation (Tian et al., 2000; Matsuno et al., 2006; Tian et al., 2007). Overexpression of ICAM-5 results in a dramatic increase in dendritic filopodia with a concomitant decrease in the density of mature mushroom spines. ICAM-5-deficient mice, on the other hand, show a decrease in filopodia numbers and an increase in spine maturation as well as an enlargement of spine heads (Matsuno et al., 2006).

Matrix metalloproteinases (MMPs) constitute a large family of zinc-dependent endopeptidases involved in many physiological and pathological processes, including extracellular matrix degradation and remodeling (McCawley and Matrisian, 2001; Sternlicht and Werb, 2001). Among known substrates are several proteins that play important roles in synaptogenesis, synaptic plasticity and long-term potentiation (LTP) (Ethell and Ethell, 2007). In the developing cerebral cortex, MMP-2 and 9 are abundantly expressed and are associated with both glial elements as well as neuronal cell bodies and dendrites (Szklarczyk et al., 2002). ICAM-5 is cleaved by multiple MMPs, including MMP-2, -9 (Tian et al., 2007) as well as MMP-3, -7 (Conant et al., 2010; Conant et al., 2011). In hippocampal neuronal cultures, NMDA or AMPA treatment induces significant release of soluble ICAM-5 (sICAM-5) fragments with an attendant reduction of membrane-bound ICAM-5 (Tian et al., 2007). It is speculated that these different fragments elicit varying downstream effects (Furutani et al., 2007). Indeed, MMP-2 and -9 mediated cleavage of ICAM-5 results in both filopodial elongation as well as spine maturation (Tian et al., 2007; Conant et al., 2011).

Given the growing evidence that MMP-mediated ICAM-5 cleavage promotes spine maturation *in vitro* (Tian et al., 2007; Wang et al., 2008; Conant et al., 2010; Conant et al., 2011; Michaluk et al., 2011), it is surprising that little is known about the ultrastructural localization of ICAM-5 *in vivo* during postnatal development. To gain an understanding of ICAM-5 regulation *in vivo*, we examined subcellular ICAM-5 expression in the visual cortex before and during the critical period for ocular dominance plasticity, a time when

synapses are prone to activity-dependent remodeling (Hensch, 2005b; Hensch, 2005a). We used immunocytochemical electron microscopy (EM) to determine ICAM-5 expression and localization within the neuropil *in vivo* in mice with and without MMP-9 expression. Specifically, we used immunoperoxidase staining with a pre-embedding approach that offers an excellent compromise between sensitivity of immunodetection and quality of ultrastructural preservation (Tremblay et al., 2010b). Our results confirm previous reports showing that ICAM-5 is primarily expressed in dendritic shafts and dendritic protrusions and additionally reveal an unexpected expression in glia. We also show changes in ICAM-5 expression in MMP-9 null animals suggesting a role for this extracellular protease in the developmental processing of ICAM-5.

Materials and Methods

Animals

Animals were treated in strict accordance with the University of Rochester Committee on Animal Resources and the 2011 NIH guide for the Care and Use of Laboratory animals. Animals were housed under a fixed 12-h light/dark cycle. For electron microscopy preparations, n=6 wild-type (WT) mice (n=3 P14; n=3 P28) and n=6 MMP-9 knock-out (KO) (B6.FVB(Cg).Mmp9tm1Tvu/J; The Jackson Laboratory; n=3 P14; n=3 P28) were anesthesized with sodium pentobarbital (150 mg/kg; i.p.) and perfused through the aortic arch with ice cold phosphate buffered saline (0.1M PBS; 0.9% NaCl in 50mM phosphate buffer [pH 7.4] followed by 3.5% acrolein in 0.1M phosphate buffer (PB). Animals were further fixed with 4% paraformaldehyde (in 0.1M PB) as detailed previously (Tremblay et al., 2010b). Brains were post-fixed for 2 hours in 4% paraformaldehyde, rinsed thoroughly in 0.05M PBS and cut at 50 μm in ice-cooled PBS on a vibratome. For standard histological comparison between WT (n=3) and ICAM-5 KO (n=3) mice (generated by gene targeting; methods described in (Nakamura et al., 2001)), were anesthetized with sodium pentobarbital (150 mg/kg; i.p.) and perfused through the aortic arch with 4% paraformaldehyde in 0.1M PBS. Brains were post-fixed for 2 hours in 4% paraformaldehyde and infiltrated with ascending concentrations of sucrose (10%, 20% and 30% in double distilled H_2O) before sectioning on a freezing sliding microtome.

Antibody Characterization

The antibodies used in this study were received as gifts or obtained from commercial sources (see Table 1).

The ICAM-5cp antibody (a gift from Dr. Y. Yoshihara; Brain Science Institute/Institute of Physical and Chemical Research, Wako City, Japan) specifically recognizes the dendrite-associated intercellular adhesion molecule, ICAM-5, restricting its expression to the telencephalon (Yoshihara et al., 1994). The antiserum was produced in rabbit, targeting the peptide sequence: AEGGAETPGT AESPADGEVF AIQLTSS which pertains to the last 17 amino acids in the C-terminus of mouse telencephalon (Yoshihara et al., 1994). To verify the specific immunoreactivity of the anti-ICAM-5cp antibody, sections from WT and ICAM-5 KO animals were processed as described below for anti-ICAM-5cp immunoperoxidase reactivity and were compared using light microscopy. The staining observed in WT mice showed the expected distribution for ICAM-5 (Yoshihara et al., 1994): it was restricted to the telencephalic region of the mouse cerebral cortex (Figure 1A) and was dense in the neocortical layers with immunoreactivity restricted primarily to the neuropil (encompassing the dendritic processes). Fiber tracts, such as the corpus callosum, remained unstained. Immunoreactivity was dense in most hippocampal layers. The hilus, dentate granular cell (dg) layer and pyramidal cell layer (pcl) remained unstained. Similarly, the thalamus remained unstained, confirming the telencephalic localization of ICAM-5

(Mori et al., 1987; Oka et al., 1990; Yoshihara et al., 1994). In comparison to WT brains, the ICAM-5 KO brain remained completely devoid of immunoreactivity, demonstrating the specificity of the antibody (Figure 1B).

The Iba-1 antibody is a well-recognized marker for microglia (Ito et al., 1998) and demonstrates specific reactivity in microglial cell bodies as well as proximal and distal processes at the light and electron microscopic levels (Trapp et al., 2007; Tremblay et al., 2010a; Lu et al., 2011). Specifically, this Iba-1 antibody was characterized in detail at the light microscopic level (Tremblay et al., 2010a) as well as in electron microscopic preparations (Tremblay et al., 2010a) in the mouse visual cortex, where the antibody failed to label non-microglial structures, such as dendritic spines and terminals. To determine antibody specificity in our study, we performed additional confirmation experiments on WT sections and processed the tissue for anti-Iba-1 immunoperoxidase reactivity. Anti-Iba-1 immunoreactivity was dense in microglial cell bodies and processes identified by their distinctive morphology whereby dense ramified processes emanate from small cell bodies distributed throughout the brain (Figure 1C). Immunoreactivity was not present in other structures and surrounding neuropil. In addition, we exposed anti-Iba-1 processed tissue to either anti-glial fibrillary acidic protein (GFAP; an astrocytic marker; Figure 1D, Table 1) or anti-neuronal nuclei (NeuN; a neuronal cell marker, Figure 1E, Table 1) and found no colocalization with anit-Iba-1 immunoreactivity, further showing the specificity of this antibody for microglia as opposed to other glial or neuronal cells.

Immunoperoxidase Reactivity for Light Microscopy and EM

Sections were immersed in 0.1% borohydride (in 0.1M PBS) for 30 minutes at room temperature (RT), washed in 0.1M PBS, and processed freely floating following a pre-embedding immunoperoxidase protocol previously described (Riad et al., 2000; Tremblay et al., 2010b).

Briefly, sections were rinsed in 0.1M PBS, followed by a 2-hour pre-incubation at RT in a blocking solution containing 5% normal goat serum and 0.5% fish gelatin. Sections were then incubated for 48-h at RT in either rabbit-anti-ICAM-5cp antibody directed against the cytoplasmic tail of mouse ICAM-5 (1:500 in blocking solution; Table 1) or rabbit anti-Iba-1 (1:1,000 in blocking solution; Table 1; Wako Pure Chemical Industries) and rinsed thoroughly in 0.1M PBS (pH 7.4). Sections were incubated for 2-hours at RT in goat anti-rabbit IgG conjugated to biotin (Jackson Immunoresearch) and with streptavidin-horseradish peroxidase (Jackson Immunoresearch) for 1-hour at RT in blocking solution. Immunoreactivity was visualized with diaminobenzidine (0.5 mg/ml) and hydrogen peroxide (0.03%) in buffer solution (DAB Peroxidase Substrate Kit; Vector Laboratories). Sections processed for fluorescent immunoreactivity experiments, were first pre-incubated in blocking solution (as detailed above) and then incubated simultaneously for 48-h at RT in a cocktail containing rabbit anti-Iba-1 and mouse anti-glial fibrillary acidic protein- Cy3 (GFAP,1:1000 in blocking solution; Table 1; Sigma) or rabbit Iba-1 and mouse anti-neuronal nuclei (NeuN; 1:500 in blocking solution; Table 1, EMD Millipore Corp). Following a thorough wash in 0.1M PBS, sections were incubated with goat anti-rabbit Alexa Fluor 488 (Invitogen) or goat anti-mouse Alexa Fluor 647 (Invitrogen).

Sections for light microscopy were mounted onto microscope slides from a 1% gelatin solution (in 99% ethanol), dehydrated in ascending concentrations of ethanol, cleared in xylene, and coverslipped with D.P.X. mounting media (Electron Microscopy Sciences [EMS]). Sections treated with immunofluorescence were coverslipped with Prolong Gold containing DAPI (Invitrogen) anti-fade mounting media.

Sections for EM were post-fixed flat in 1% osmium tetroxide and dehydrated in ascending concentrations of ethanol. They were treated with propylene oxide, impregnated in Durcupan (EMS) overnight at RT, mounted between ACLAR embedding films (EMS), and cured at 55°C for 48-hours. Areas of the primary visual cortex (V1, Layer 2), at the level approximating the transverse planes A +0.16 to A +0.72 (Franklin and Paxinos, 2008), were excised in a trapezoid shape from the embedding films in a selected orientation to accurately determine the pial surface during ultrathin sectioning and re-embedded at the tip of resin blocks. Ultrathin sections (60–80 nm; evidenced by the sections silver sheen) were cut with an ultramicrotome (Reichert Ultracut E) and collected on bare square-mesh grids.

Double Immunoperoxidase and Immunogold Reactivity for EM

Selected brain sections were dually stained for ICAM-5 and Iba-1 following a protocol previously described in detail (Bouvier et al., 2008). Briefly, sections were processed for Iba-1 immunoperoxidase staining (see above) through the diaminobenzidine (DAB) visualization step. Sections were then rinsed in 0.1M PBS, followed by a 2-hour preincubation at room temperature in a blocking solution containing 5% normal goat serum and 0.5% fish gelatin. Sections were then incubated for 48-h at room temperature in rabbit-anti-ICAM-5cp antibody. Sections were incubated for 2-hours at RT in goat anti-rabbit IgG conjugated to biotin (Jackson Immunoresearch) followed by a thorough wash in 0.1M PBS. Sections were then incubated in streptavidin nanogold (1:500, Nanoprobes #2016; Yaphank, NY) for 2 hours. Sections were silver enhanced using IntenSE™ Silver Enhancement Reagents #RPN491 (per kit instructions, G.E. Healthcare; Piscataway, NJ). Sections were postfixed flat in 1% osmium tetroxide and dehydrated in ascending concentrations of ethanol and processed for EM examination (see above). To test the specificity of our reactions and to determine the best visualization pairings for our two antibodies, a variety of control experiments were performed in parallel. These experiments included: anti-Iba-1 visualized with DAB only, anti-Iba-1 visualized with gold only, anti-ICAM-5 visualized with DAB only, anti-ICAM-5 visualized with gold only, anti-Iba-1 visualized with DAB and anti-ICAM-5 visualized with gold (dual reactivity), and anti-Iba-1 visualized with gold and anti-ICAM-5 visualized with DAB (dual reactivity).

Light and Epifluorescent Microscopy Imaging

Light and epifluorescent microscope pictures of ICAM-5 immunoreactivity in ICAM-5 KO and WT mice and Iba-1 dual labeled tissue were taken on a BX51 Olympus Scope at 10X magnification (UPlanFL N; 10X/0.30; Olympus), 20X (UPlanFL N; 20X/0.50; Olympus) and 60X (UPlanFL N; 60X/0.90; Olympus) mounted with a SPOT Pursuit RT color digital camera (Diagnostic Instruments).

EM Imaging and Data Analysis

Eighty pictures were randomly taken at 40,000X in layer II of V1 (approximately 10 microns from the pial surface) in each animal at the tissue-resin border corresponding to a total surface of ~ 1,000 μm^2 of neuropil per animal (as in (Tremblay et al., 2007; Bouvier et al., 2008; Tremblay et al., 2009; Bouvier et al., 2010; Kelly et al., 2010; Tremblay et al., 2010a; Mortillo et al., 2012), among others). Images were captured on a Hitachi 7650 Transmission Electron Microscope using a Gatan 11 megapixel Erlangshen digital camera and Digitalmicrograph software. TIFF images were exported into Adobe Photoshop (CS5.5) and adjusted for brightness and contrast in preparation for analysis. Cellular profiles were identified using a series of criteria previously defined in single-ultrathin sections (Peters et al., 1991; Tremblay et al., 2009; Tremblay et al., 2010a; Lu et al., 2011). All ICAM-5 labeled structures were classified into the following categories: *dendrite*, *dendritic protrusion (including dendritic spines and putative filopodia)*, axon *terminal*, and glial

elements (including *microglia* and *astrocytes)*. We conservatively classified all the subcellular profiles that were difficult to identify as “unknown”.

In several instances, the density of ICAM-5 immunoreactivity obscured some of the intracellular organelles and defining characteristics. When this happened, we relied on the visible defining features, such as contours made by the profiles and ultrastructural relationships with neighboring profiles to aid in our classification. Furthermore, even though ICAM-5 immunoreactivity was very dense in some profiles, organelles such as mitochondria and endoplasmic reticulum stretches were often visible through the DAB reactivity; while cytoskeletal elements such as microtubules were emphasized by the DAB (see Figure 2B–D; Figure 4A).

Dendrite—Dendritic shafts cut longitudinally were recognized by their irregular contours, elongated mitochondria in parallel with their central axis, frequent protuberances (spines, filopodia, small branches), and synaptic contacts with axon terminals (see below). When cut transversally, dendritic shafts were identified by their rounded morphology, frequent occurrence of mitochondria and microtubules, and they were distinguished from unmyelinated axons by their larger diameter.

Dendritic protrusion—Dendritic spines and filopodia cut longitudinally often protruded from dendritic shafts, displayed rounded morphologies and were free of mitochondria. Dendritic spines were characterized primarily by the presence of electron-dense accumulations (postsynaptic densities) at synaptic contact sites with axon terminals. Compared with dendritic spines, putative filopodia cut longitudinally were longer, displayed smaller heads with pointy rather than bulbous extremities, and were typically devoid of postsynaptic densities (Fiala et al., 1998). When cut transversally, putative filopodia were distinguished from small unmyelinated axons based on the absence of fascicles (small axons tend to travel through neuropil in bundles in which they are arranged parallel to each other (Peters et al., 1991)) and from glial profiles based on the criteria described below. Because the DAB reaction product could obscure postsynaptic densities when particularly dense, making it difficult to discriminate small dendritic spines from filopodia, the two types of dendritic protrusions were grouped into one category

Axon terminal—Axonal terminals were distinguished from other subcellular profiles based primarily on the presence of 40 nm diameter synaptic vesicles, with rounded to elongated morphologies, but also of synaptic contacts with dendritic shafts and protrusions (dendritic spines and filopodia). Axon terminals generally contained mitochondria.

Glia—Protoplasmic astrocytes were recognized as electron-lucent structures seen to encase and wrap around other neuropil structures. As a result, astrocytes maintained irregular and angular shapes, distinguishing them from other neuronal profiles having a characteristic rounded shape. Microglial processes displayed irregular contours with obtuse angles, distinctive long stretches of endoplasmic reticulum visible through the DAB staining, electron-dense cytoplasm, numerous large vesicles, occasional multi-vesicular bodies, vacuoles or cellular inclusions, and distinctive surrounding extracellular space (Tremblay et al., 2010a; Lu et al., 2011; Tremblay et al., 2012), distinguishing them from astrocytes, oligodendrocytes or NG2-positive glial cells. Glial structures (astrocytes and microglia) were grouped into one category for this study.

Quantitative Analysis—To obtain the average density of ICAM-5 labeled elements, the number of ICAM-5 immunopositive elements was quantified in an area of 1,000 μm^2 total neuropil (i.e. excluding cell bodies and blood vessels) per animal. The value for each

individual animal was averaged across each condition. To determine the percentage of ICAM-5 labeled elements, all ICAM-5 labeled elements were classified into the previously defined categories and the total number of ICAM-5 labeled elements for each category was divided by the total number of labeled elements in each animal and averaged for all animals in each condition.

Statistics

Analysis was performed with Prism 5 software (GraphPad Software). All values reported in the text are mean ± standard error of the mean (SEM). For all statistical tests, significance was set to $p<0.05$. 'Percent ICAM-5 Labeled Elements' and 'Density ICAM-5 Labeled Elements" were analyzed using a 2-way ANOVA with Bonferroni multiple comparisons post-hoc tests. Sample size *(n)* represents individual animals.

Results

Ultrastructural distribution of ICAM-5

To provide a detailed view of the distribution of ICAM-5 in the mouse visual cortex, we performed EM analysis in cortical layer 2 at P14, a period of robust synaptogenesis (Li et al., 2010) and P28, an adolescent period when synaptogenesis is largely complete but neuronal circuitry continues to mature through the elimination of synapses (Zuo et al., 2005). At the light microscopic level, anti-ICAM-5 immunoreactivity was found in cell bodies and neuropil predominately within the telencephalic structures of the neocortex (see Figure 1A). At the EM levels we found that ICAM-5 reactivity predominates in dendritic elements at P14 and P28 (Figure 2A–D), including dendritic protrusions and shafts in accordance with previous findings in vitro (Oka et al., 1990; Murakami et al., 1991; Yoshihara et al., 1994; Benson et al., 1998; Sakurai et al., 1998). Quantitative analysis showed that the average density of ICAM-5-labeled structures was higher at P14 compared to P28 (P14=4.617 ± 0.394; P28=2.847 ±0.211; $p<0.05$; data not shown), further corroborating previous findings that ICAM-5 is developmentally regulated (Mori et al., 1987; Imamura et al., 1990; Yoshihara et al., 1994; Matsuno et al., 2006; Tian et al., 2007).

We performed quantitative analysis detailing the percentage of different subcellular structures expressing ICAM-5 (Figure 2E, 2F). At P14, immunoreactivity was predominantly found in dendritic protrusions, including synaptic and non-synaptic structures as well as in dendrites (Figure 2E). Surprisingly, we also detected immunoreactivity in glial elements. ICAM-5 was completely absent from axonal terminals, supporting the findings that ICAM-5 is restricted to the somatodendritic compartment and confirming the specificity of the immunostaining (Oka et al., 1990; Murakami et al., 1991; Benson et al., 1998; Sakurai et al., 1998). By P28, ICAM-5 expression showed an evident shift from dendritic protrusions (Figure 2E; P14 vs, P28 dendritic protrusions, $p<0.01$) to dendritic shafts (Figure 2E, P14 vs. P28 dendrite expression, $p< 0.001$). Interestingly, when we considered only dendritic spines which contained the hallmarks of a functional synapse (a postsynaptic density, accumulations of vesicles in opposing axonal terminal), we observed low levels of labeling and no significant shift in the percentage of labeled structures between P14 and P28 (labeled density: P14: 8.230 ± 4.354 per 1000 μm^2 of neuropil/animal; P28: 2.903 ± 0.875 per 1000 μm^2 of neuropil/animal, $t=0.794$, $p>0.05$), suggesting that functional spines are unlikely to contain ICAM-5 at any age. Labeled glia still comprised a small but significant percentage of labeled elements. We analyzed the density of individual ICAM-5 labeled elements at the two ages and determined that this shift was mediated by the loss of ICAM-5 labeled dendritic protrusions at P28 (Figure 2F; $p<0.05$;). At P28, the density of ICAM-5 labeled dendrites was increased although this effect did not reach statistical significance.

ICAM-5 expression in microglial elements

While ICAM-5 is generally thought to be restricted to neuronal dendrites, we noted ICAM-5 immunoreactivity in glial elements in this study. Because some of the immunoreactive profiles resembled the microglial structures we have recently described in EM analyses (Tremblay et al., 2010a), we confirmed the localization of ICAM-5 in microglial processes by performing double immunoperoxidase DAB immunoreactivity for Iba-1 and immunogold reactivity for ICAM-5 (Figure 3A–D). As expected the DAB staining for Iba-1 was found throughout microglial structures, including cell bodies, proximal and distal processes. The immunogold reactivity for ICAM-5 also showed the expected distribution in neuronal cell bodies, dendrites, dendritic protrusions and glial profiles, including Iba-1 labeled microglial elements (Figure 3A–D). As the immunogold labeling affords a precise localization, this analysis also revealed that ICAM-5 predominantly localizes to the plasma membrane of neuronal and glial profiles (see Figure 3E for examples in somatodendritic compartments) (Oka et al., 1990; Murakami et al., 1991; Benson et al., 1998; Sakurai et al., 1998).

MMP-9 regulates ICAM-5 Localization

ICAM-5 is cleaved by multiple MMPs (Tian et al., 2007; Conant et al., 2010; Conant et al., 2011), including MMP-2, -3, -7 and -9, in an activity-dependent manner *in vitro* (Tian et al., 2007), although this has not been studied *in vivo*. We hypothesized that the absence of MMP-9 would alter the expression of ICAM-5 in developing visual cortex. To determine the degree by which ICAM-5 expression patterns are regulated by MMP-9, we analyzed the ultrastructural distribution of ICAM-5 at P14 and P28 in the visual cortex of MMP-9 KO mice.

MMP-9 KO mice were not qualitatively distinguishable from WT control mice in gross anatomical or ultrastructural comparisons although minor defects in the cortex, hippocampus and cerebellum have been described (Vaillant et al., 2003; Tian et al., 2007). Pre-embedding immunoperoxidase EM of MMP-9 cortex revealed ICAM-5 immunoreactivity in dendritic compartments at P14 (Figure 4A) and P28 (Figure 4B). Interestingly, while we found a developmental regulation of ICAM-5 expression in WT animals from P14 to P28, the average ICAM-5 labeling density did not change significantly from P14 to P28 in MMP-9 KO mice (P14=2.459 ±0.414; P28=2.355 ±0.558; $p<0.05$). Also, whereas ICAM-5 was distributed between both dendritic shafts and dendritic protrusions at P14 in WT mice (Figure 2A), in MMP-9 KO mice ICAM-5 immunoreactivity was most prevalent in protrusions (Figure 4C; Table 2; $p<0.01$) with a small level of immunoreactivity in dendritic shafts (Figure 4C) and glia (Figure 4C). By P28, however, the ICAM-5 expression profile was altered from that observed in WT animals. A significant decrease in the percentage of labeled dendritic shafts was observed (P28 WT vs MMP-9 KO Table 2, $p<0.001$), and the developmental shift from protrusion towards dendritic shaft labeling was not evident. Dendritic protrusions (Figure 4C) continued to make up the largest percentage of immunoreactive elements at P28 in MMP-9 KO mice. Immunoreactive protrusions that contained evidence of functional synapses (a postsynaptic density, accumulations of vesicles in opposing axon terminal), however, appeared to be more prevalent in MMP-9 KO animals at both ages (P14 WT: 8.230 ± 4.354; KO: 17.720 ± 4.111, $p<0.05$; P28 WT: 2.903± 0.875; KO: 33.423 ± 10.793, $p<0.05$), suggesting that ICAM-5 may not be appropriately limited from synaptic structures. Glial immunoreactivity was similar to that in control cortex (Figure 4D). Again no imunoreactivity within presynaptic terminals was observed at any age.

Comparison of the density of ICAM-5 labeled elements in MMP-9 mice at P14 and P28 showed similar densities for all elements between these ages (Figure 4D) and confirmed the high degree of immunoreactivity in dendritic protrusions at both P14 and P28. We found a surprisingly low density of labeled dendritic shafts which did not change with age.

Discussion

Given the importance of ICAM-5 signaling for spine maturation and circuit development it is surprising that little information is available as to how ICAM-5 subcellular localization is regulated in the intact developing brain. To determine the localization and regulation of ICAM-5 expression during development *in vivo*, we used electron microscopy to investigate the ultrastructural environment of ICAM-5 labeled elements in the mouse primary visual cortex and determine the effects of MMP-9 on ICAM-5 distribution in MMP-9 KO mice. We show that in the absence of MMP-9, ICAM-5 remains in dendritic protrusions from P14 to P28 without undergoing the normal developmental shift towards more prominent expression in dendritic shafts. Additionally, ICAM-5 appears to also be expressed in functional dendritic spines in MMP-9 KO mice, suggesting a dysregulation of ICAM5 distribution in the absence of MMP9 activity during development.

ICAM-5 expression switches from dendritic protrusions to dendritic shafts during development

To investigate the ultrastructural localization of ICAM-5 we performed pre-embedding immunoperoxidase histochemistry for ICAM-5 in mouse visual cortex at P14, a period of intense synaptogenesis (Li et al., 2010) and P28, an adolescent period when synaptogenesis is largely complete but circuitry matures through the elimination of synapses (Zuo et al., 2005). We show that ICAM-5 expression is evident in dendritic protrusions at P14 and that this expression profile shifts significantly to dendritic shafts by P28. These findings are consistent with previous reports that suggest a developmental significance of ICAM-5 in emergent dendritic structures (Matsuno et al., 2006; Tian et al., 2007) where ICAM-5 expression is enhanced in early development and limited to immature structures such as filopodia. Because it was sometimes difficult to discriminate immature dendritic spines from filopodia at the EM level without three dimensional reconstructions, especially when the DAB reaction product was obscuring postsynaptic densities, we chose to combine dendritic protrusions into one category. However, it is interesting to note that when we separated out protrusions that had clear hallmarks of a synaptic connections such as postsynaptic densities (dendritic spines), we found that these had a very low level of ICAM-5 labeling at either age. This further suggests that the developmental switch described here is driven by changes in ICAM-5 expression within immature dendritic protrusions (putative filopodia and immature dendritic spines).

While our findings support the previous *in vitro* observations, they are the first documentation of ultrastructural localization of ICAM-5 during development *in vivo*, and are valuable as they provide a quantitative view of ICAM-5 subcellular distribution. Although other groups have used EM in murine hippocampus (Sakurai et al., 1998; Nakamura et al., 2001) and rabbit olfactory bulb (Murakami et al., 1991) they documented only the qualitative distribution of ICAM-5 in somatic and dendritic membrane fractions and primarily focused on adulthood. The change in ICAM-5 localization during the period from P14 to P28 in WT suggests strongly that ICAM-5 is developmentally regulated during this plastic period of synaptic development within visual cortex.

Interestingly, we found a surprisingly large fraction of ICAM-5-labeled elements to be of glial origin at both ages, suggesting that ICAM-5 may have a role beyond dendritic regulation and synaptic maturation. Using double immunoperoxidase histochemistry and EM analysis for the microglial marker, Iba-1, and ICAM-5, we showed a specific localization of Iba-1 to microglial elements with ICAM-5 localized to the microglial plasma membrane, suggesting that at least some of the ICAM-5-labeled glial profiles were microglial elements. While these findings suggest that microglia may express ICAM-5 it is also possible that soluble ICAM-5 cleaved by MMP's is binding to a receptor in the

microglial membrane. Indeed, microglia have been shown to express LFA-1 (leukocyte specific β_2-integrin, CD11b/CD18, $\alpha_L\beta_2$) which is a binding partner of ICAM-5 (Gahmberg, 1997; Gahmberg et al., 1997; Tian et al., 1997; Mizuno et al., 1999; Gahmberg et al., 2008). Furthermore, ICAM-5 binding to LFA-1 *in vitro* has been shown to induce cell spreading of microglia (Mizuno et al., 1999) suggesting an integral role for ICAM-5 in microglial function. Future studies will be needed to characterize the intriguing role of ICAM-5 in glia.

MMP-9 deficiency alters ICAM-5 distribution in dendritic protrusions during development

We show that ICAM-5 expression is retained in dendritic protrusions from P14 to P28 in the visual cortex of MMP-9 KO mice. ICAM-5 expression does not increase in dendritic shafts by P28 as seen in age-matched WT mice, but remains in synaptic structures as they mature, as evidenced by the significant immunoreactivity observed in dendritic spines with clearly identified synapses. These findings provide *in-vivo* evidence that MMP-9 is critical for the mature distribution of ICAM-5 and its exclusion from synapses. While it is unclear what mechanism drives the ICAM-5 expression profile to switch from a dendritic protrusion to a primarily shaft localization, it is possible that MMP-9 may be involved in the lateral diffusion of ICAM-5 out of filopodia and spines and into dendritic shaft membranes, or that MMP-9-mediated cleavage affects the localization of newly synthesized ICAM-5 in protrusions. Indeed, ICAM-5 has different binding partners depending on its subcellular localization. ICAM-5 interacts with the actin cytoskeleton within dendritic filopodia (Nyman-Huttunen et al., 2006; Furutani et al., 2007; Tian et al., 2007) via phosphorylated ERM (ezrin/radixin/moesin) proteins, but dendritic ICAM-5 binds directly to α-actinin in the absence of phosphorylated ERMs (Nyman-Huttunen et al., 2006). Interestingly, it was previously shown that broad spectrum MMP inhibitors blocked the NMDA-induced cleavage of ICAM-5 along dendritic shafts but not in thin spines possibly due to a difference is MMP susceptibility in spine heads versus dendritic shafts (Tian et al., 2007). Our finding that ICAM-5 is retained in dendritic protrusions from P14 to P28 in MMP-9 KO mice seems to partially contradict this finding. If filopodia or thin spines were less susceptible to MMP-9 deficiency, we would expect to see a decreased expression in dendritic protrusions (since ICAM-5 would be cleaved and removed) with age. Instead, we see low ICAM-5 expression in dendritic shafts from P14 to P28 with high levels retained in protrusions as they develop in the absence of MMP-9.

ICAM-5 shedding has been shown to be blocked by application of inhibitors to MMP-2, -9 (Tian et al., 2007), -3, and -7 (Conant et al., 2010) implicating a degree of redundancy in protease activity. Indeed, Tian et. al. (2007) showed that single knockout of MMP-2 or -9 resulted in a significant increase in full-length ICAM-5 expression, however the double MMP-2/-9 mutant showed a decrease in full-length ICAM-5. Compensatory expression of similar acting (or redundant) proteases is likely to be responsible (Sekine-Aizawa et al., 2001; Greenlee et al., 2007), and it has been shown that deleting one MMP can lead to a compensatory upregulation of another (Esparza et al., 2004; Tian et al., 2007). While such compensatory mechanisms are likely at play in the MMP-9 KO mouse, our findings suggest that MMP-9 has a unique role in mediating the developmental shift in ICAM-5 localization.

ICAM-5 and synaptic maturation

A first interpretation of our data may seem to argue against the prevailing model that ICAM-5 cleavage allows the formation of a mature synapse, since MMP-9 KO mice appear to have ICAM-5 labeling in dendritic protrusions bearing functional synapses. However, alternate interpretations may explain the discrepancy (see Figure 5). ICAM-5 is cleaved at multiple sites by a variety of MMPs, thus ICAM-5 cleavage by MMPs other than MMP-9 may be sufficient to trigger a maturation cascade without removing the ICAM-5 protein from the synaptic structure. In fact soluble cleavage products such as sICAM-5 have been

shown to bind β-1 integrins resulting in cofilin phosphorylation and spine growth (Conant et al., 2011; Ning et al., 2013), suggesting a possible compensational mechanism provided by β-1 integrins. Alternatively, the observed ICAM-5 immunoreactivity in dendritic protrusions at P28 might suggest increased immaturity of the MMP-9 KO cortex at this age. Lack of appropriate ICAM-5 cleavage may result in more immature, weaker protrusions due to retained ICAM-5 in synaptic structures. Future experiments detailing the morphology, density or synaptic strength of visual cortical synapses in MMP9 KO mice would be required to explore this possibility.

In summary, using ultrastructural analysis, we have shown that ICAM-5 expression is relegated primarily to dendritic protrusions during early periods of synaptogenesis (P14) in WT mice, but that this expression shifts to dendritic shafts by P28, supporting a role for ICAM-5 in the maturation of synaptic structure. MMP-9 KO mice show normal ICAM-5 expression at P14, but fail to shift expression to dendritic shafts at P28 and retain immunoreactivity in dendritic protrusions. We conclude that MMP-9 regulates the cleavage of ICAM-5 which in turn determines its subcellular localization during development.

Acknowledgments

We'd like to thank Karen Bentley and Gayle Schneider and the entire URMC Electron Microscope Research Core for their expert training and guidance. This work is supported by the National Institutes of Health (NIH) grants EY019277 (A.K.M.) and T32 ES 7026-34 (E.A.K), National Eye Institute (NEI) grant EY013319 (E.A.K), Fonds de Recherche en Santé du Québec (FRSQ) and Canadian Institutes of Health Research (CIHR) fellowships (M.E.T), the Finnish Medical Association, the Sigrid Jusélius Foundation and the Liv och Hälsa Foundation (CGG) and Academy of Finland and Magnus Ehrnrooth Fountation (L.T).

Literature Cited

Benson DL, Yoshihara Y, Mori K. Polarized distribution and cell type-specific localization of telencephalin, an intercellular adhesion molecule. J Neurosci Res. 1998; 52(1):43–53. [PubMed: 9556028]

Bouvier D, Corera AT, Tremblay ME, Riad M, Chagnon M, Murai KK, Pasquale EB, Fon EA, Doucet G. Pre-synaptic and post-synaptic localization of EphA4 and EphB2 in adult mouse forebrain. Journal of neurochemistry. 2008; 106(2):682–695. [PubMed: 18410519]

Bouvier D, Tremblay ME, Riad M, Corera AT, Gingras D, Horn KE, Fotouhi M, Girard M, Murai KK, Kennedy TE, McPherson PS, Pasquale EB, Fon EA, Doucet G. EphA4 is localized in clathrin-coated and synaptic vesicles in adult mouse brain. Journal of neurochemistry. 2010; 113(1):153–165. [PubMed: 20067584]

Conant K, Lonskaya I, Szklarczyk A, Krall C, Steiner J, Maguire-Zeiss K, Lim ST. Methamphetamine-associated cleavage of the synaptic adhesion molecule intercellular adhesion molecule-5. Journal of neurochemistry. 2011; 118(4):521–532. [PubMed: 21166806]

Conant K, Wang Y, Szklarczyk A, Dudak A, Mattson MP, Lim ST. Matrix metalloproteinase-dependent shedding of intercellular adhesion molecule-5 occurs with long-term potentiation. Neuroscience. 2010; 166(2):508–521. [PubMed: 20045450]

Esparza J, Kruse M, Lee J, Michaud M, Madri JA. MMP-2 null mice exhibit an early onset and severe experimental autoimmune encephalomyelitis due to an increase in MMP-9 expression and activity. FASEB journal: official publication of the Federation of American Societies for Experimental Biology. 2004; 18(14):1682–1691. [PubMed: 15522913]

Ethell IM, Ethell DW. Matrix metalloproteinases in brain development and remodeling: synaptic functions and targets. J Neurosci Res. 2007; 85(13):2813–2823. [PubMed: 17387691]

Franklin, K.; Paxinos, G. The mouse brain in stereotaxic coordinates. New York: Academic Press; 2008. p. 216

Furutani Y, Matsuno H, Kawasaki M, Sasaki T, Mori K, Yoshihara Y. Interaction between telencephalin and ERM family proteins mediates dendritic filopodia formation. J Neurosci. 2007; 27(33):8866–8876. [PubMed: 17699668]

Gahmberg CG. Leukocyte adhesion: CD11/CD18 integrins and intercellular adhesion molecules. Current opinion in cell biology. 1997; 9(5):643–650. [PubMed: 9330867]

Gahmberg CG, Tian L, Ning L, Nyman-Huttunen H. ICAM-5--a novel two-facetted adhesion molecule in the mammalian brain. Immunol Lett. 2008; 117(2):131–135. [PubMed: 18367254]

Gahmberg CG, Tolvanen M, Kotovuori P. Leukocyte adhesion--structure and function of human leukocyte beta2-integrins and their cellular ligands. European journal of biochemistry/FEBS. 1997; 245(2):215–232. [PubMed: 9151947]

Greenlee KJ, Werb Z, Kheradmand F. Matrix metalloproteinases in lung: multiple, multifarious, and multifaceted. Physiological reviews. 2007; 87(1):69–98. [PubMed: 17237343]

Hensch TK. Critical period mechanisms in developing visual cortex. Current topics in developmental biology. 2005a; 69:215–237. [PubMed: 16243601]

Hensch TK. Critical period plasticity in local cortical circuits. Nature reviews Neuroscience. 2005b; 6(11):877–888.

Imamura K, Mori K, Oka S, Watanabe Y. Variations by layers and developmental changes in expression of telencephalin in the visual cortex of cat. Neuroscience letters. 1990; 119(1):118–121. [PubMed: 2097574]

Ito D, Imai Y, Ohsawa K, Nakajima K, Fukuuchi Y, Kohsaka S. Microglia-specific localisation of a novel calcium binding protein, Iba1. Brain research Molecular brain research. 1998; 57(1):1–9. [PubMed: 9630473]

Kelly EA, Tremblay ME, McCasland JS, Majewska AK. Postsynaptic deregulation in GAP-43 heterozygous mouse barrel cortex. Cereb Cortex. 2010; 20(7):1696–1707. [PubMed: 19915093]

Larson RS, Springer TA. Structure and function of leukocyte integrins. Immunological reviews. 1990; 114:181–217. [PubMed: 2196220]

Li M, Cui Z, Niu Y, Liu B, Fan W, Yu D, Deng J. Synaptogenesis in the developing mouse visual cortex. Brain research bulletin. 2010; 81(1):107–113. [PubMed: 19751806]

Lu SM, Tremblay ME, King IL, Qi J, Reynolds HM, Marker DF, Varrone JJ, Majewska AK, Dewhurst S, Gelbard HA. HIV-1 Tat-induced microgliosis and synaptic damage via interactions between peripheral and central myeloid cells. PloS one. 2011; 6(9):e23915. [PubMed: 21912650]

Matsuno H, Okabe S, Mishina M, Yanagida T, Mori K, Yoshihara Y. Telencephalin slows spine maturation. J Neurosci. 2006; 26(6):1776–1786. [PubMed: 16467526]

McCawley LJ, Matrisian LM. Matrix metalloproteinases: they're not just for matrix anymore! Current opinion in cell biology. 2001; 13(5):534–540. [PubMed: 11544020]

Michaluk P, Wawrzyniak M, Alot P, Szczot M, Wyrembek P, Mercik K, Medvedev N, Wilczek E, De Roo M, Zuschratter W, Muller D, Wilczynski GM, Mozrzymas JW, Stewart MG, Kaczmarek L, Wlodarczyk J. Influence of matrix metalloproteinase MMP-9 on dendritic spine morphology. J Cell Sci. 2011; 124(Pt 19):3369–3380. [PubMed: 21896646]

Mitsui S, Saito M, Hayashi K, Mori K, Yoshihara Y. A novel phenylalanine-based targeting signal directs telencephalin to neuronal dendrites. J Neurosci. 2005; 25(5):1122–1131. [PubMed: 15689548]

Mizuno T, Yoshihara Y, Kagamiyama H, Ohsawa K, Imai Y, Kohsaka S, Mori K. Neuronal adhesion molecule telencephalin induces rapid cell spreading of microglia. Brain Res. 1999; 849(1–2):58–66. [PubMed: 10592287]

Mori K, Fujita SC, Watanabe Y, Obata K, Hayaishi O. Telencephalon-specific antigen identified by monoclonal antibody. Proceedings of the National Academy of Sciences of the United States of America. 1987; 84(11):3921–3925. [PubMed: 3295872]

Mortillo S, Elste A, Ge Y, Patil SB, Hsiao K, Huntley GW, Davis RL, Benson DL. Compensatory redistribution of neuroligins and N-cadherin following deletion of synaptic beta1-integrin. The Journal of comparative neurology. 2012; 520(9):2041–2052. [PubMed: 22488504]

Murakami F, Tada Y, Mori K, Oka S, Katsumaru H. Ultrastructural localization of telencephalin, a telencephalon-specific membrane glycoprotein, in rabbit olfactory bulb. Neurosci Res. 1991; 11(2):141–145. [PubMed: 1717905]

Nakamura K, Manabe T, Watanabe M, Mamiya T, Ichikawa R, Kiyama Y, Sanbo M, Yagi T, Inoue Y, Nabeshima T, Mori H, Mishina M. Enhancement of hippocampal LTP, reference memory and

sensorimotor gating in mutant mice lacking a telencephalon-specific cell adhesion molecule. The European journal of neuroscience. 2001; 13(1):179–189. [PubMed: 11135016]

Ning L, Tian L, Smirnov S, Vihinen H, Llano O, Vick K, Davis RL, Rivera C, Gahmberg CG. Interactions between ICAM-5 and beta1 integrins regulate neuronal synapse formation. J Cell Sci. 2013; 126(Pt 1):77–89. [PubMed: 23015592]

Nyman-Huttunen H, Tian L, Ning L, Gahmberg CG. alpha-Actinin-dependent cytoskeletal anchorage is important for ICAM-5-mediated neuritic outgrowth. J Cell Sci. 2006; 119(Pt 15):3057–3066. [PubMed: 16820411]

Oka S, Mori K, Watanabe Y. Mammalian telencephalic neurons express a segment-specific membrane glycoprotein, telencephalin. Neuroscience. 1990; 35(1):93–103. [PubMed: 2359499]

Peters, A.; Palay, S.; Webster, H. The fine structure of the nervous system: The neurons and supporting cells. Philadelphia: W.B. Saunders; 1991.

Riad M, Garcia S, Watkins KC, Jodoin N, Doucet E, Langlois X, el Mestikawy S, Hamon M, Descarries L. Somatodendritic localization of 5-HT1A and preterminal axonal localization of 5-HT1B serotonin receptors in adult rat brain. The Journal of comparative neurology. 2000; 417(2): 181–194. [PubMed: 10660896]

Sakurai E, Hashikawa T, Yoshihara Y, Kaneko S, Satoh M, Mori K. Involvement of dendritic adhesion molecule telencephalin in hippocampal long-term potentiation. Neuroreport. 1998; 9(5): 881–886. [PubMed: 9579684]

Sekine-Aizawa Y, Hama E, Watanabe K, Tsubuki S, Kanai-Azuma M, Kanai Y, Arai H, Aizawa H, Iwata N, Saido TC. Matrix metalloproteinase (MMP) system in brain: identification and characterization of brain-specific MMP highly expressed in cerebellum. The European journal of neuroscience. 2001; 13(5):935–948. [PubMed: 11264666]

Sternlicht MD, Werb Z. How matrix metalloproteinases regulate cell behavior. Annual review of cell and developmental biology. 2001; 17:463–516.

Szklarczyk A, Lapinska J, Rylski M, McKay RD, Kaczmarek L. Matrix metalloproteinase-9 undergoes expression and activation during dendritic remodeling in adult hippocampus. J Neurosci. 2002; 22(3):920–930. [PubMed: 11826121]

Tian L, Nyman H, Kilgannon P, Yoshihara Y, Mori K, Andersson LC, Kaukinen S, Rauvala H, Gallatin WM, Gahmberg CG. Intercellular adhesion molecule-5 induces dendritic outgrowth by homophilic adhesion. J Cell Biol. 2000; 150(1):243–252. [PubMed: 10893271]

Tian L, Stefanidakis M, Ning L, Van Lint P, Nyman-Huttunen H, Libert C, Itohara S, Mishina M, Rauvala H, Gahmberg CG. Activation of NMDA receptors promotes dendritic spine development through MMP-mediated ICAM-5 cleavage. J Cell Biol. 2007; 178(4):687–700. [PubMed: 17682049]

Tian L, Yoshihara Y, Mizuno T, Mori K, Gahmberg CG. The neuronal glycoprotein telencephalin is a cellular ligand for the CD11a/CD18 leukocyte integrin. J Immunol. 1997; 158(2):928–936. [PubMed: 8993013]

Trapp BD, Wujek JR, Criste GA, Jalabi W, Yin X, Kidd GJ, Stohlman S, Ransohoff R. Evidence for synaptic stripping by cortical microglia. Glia. 2007; 55(4):360–368. [PubMed: 17136771]

Tremblay ME, Lowery RL, Majewska AK. Microglial interactions with synapses are modulated by visual experience. PLoS biology. 2010a; 8(11):e1000527. [PubMed: 21072242]

Tremblay ME, Riad M, Bouvier D, Murai KK, Pasquale EB, Descarries L, Doucet G. Localization of EphA4 in axon terminals and dendritic spines of adult rat hippocampus. The Journal of comparative neurology. 2007; 501(5):691–702. [PubMed: 17299751]

Tremblay ME, Riad M, Chierzi S, Murai KK, Pasquale EB, Doucet G. Developmental course of EphA4 cellular and subcellular localization in the postnatal rat hippocampus. The Journal of comparative neurology. 2009; 512(6):798–813. [PubMed: 19086003]

Tremblay ME, Riad M, Majewska A. Preparation of mouse brain tissue for immunoelectron microscopy. Journal of visualized experiments: JoVE. 2010b; (41)

Tremblay ME, Zettel ML, Ison JR, Allen PD, Majewska AK. Effects of aging and sensory loss on glial cells in mouse visual and auditory cortices. Glia. 2012; 60(4):541–558. [PubMed: 22223464]

Vaillant C, Meissirel C, Mutin M, Belin MF, Lund LR, Thomasset N. MMP-9 deficiency affects axonal outgrowth, migration, and apoptosis in the developing cerebellum. Molecular and cellular neurosciences. 2003; 24(2):395–408. [PubMed: 14572461]

Wang XB, Bozdagi O, Nikitczuk JS, Zhai ZW, Zhou Q, Huntley GW. Extracellular proteolysis by matrix metalloproteinase-9 drives dendritic spine enlargement and long-term potentiation coordinately. Proceedings of the National Academy of Sciences of the United States of America. 2008; 105(49):19520–19525. [PubMed: 19047646]

Yoshihara Y, Mori K. Telencephalin: a neuronal area code molecule? Neurosci Res. 1994; 21(2):119–124. [PubMed: 7724062]

Yoshihara Y, Oka S, Nemoto Y, Watanabe Y, Nagata S, Kagamiyama H, Mori K. An ICAM-related neuronal glycoprotein, telencephalin, with brain segment-specific expression. Neuron. 1994; 12(3):541–553. [PubMed: 7794412]

Zhang H, Casasnovas JM, Jin M, Liu JH, Gahmberg CG, Springer TA, Wang JH. An unusual allosteric mobility of the C-terminal helix of a high-affinity alphaL integrin I domain variant bound to ICAM-5. Molecular cell. 2008; 31(3):432–437. [PubMed: 18691975]

Zuo Y, Yang G, Kwon E, Gan WB. Long-term sensory deprivation prevents dendritic spine loss in primary somatosensory cortex. Nature. 2005; 436(7048):261–265. [PubMed: 16015331]

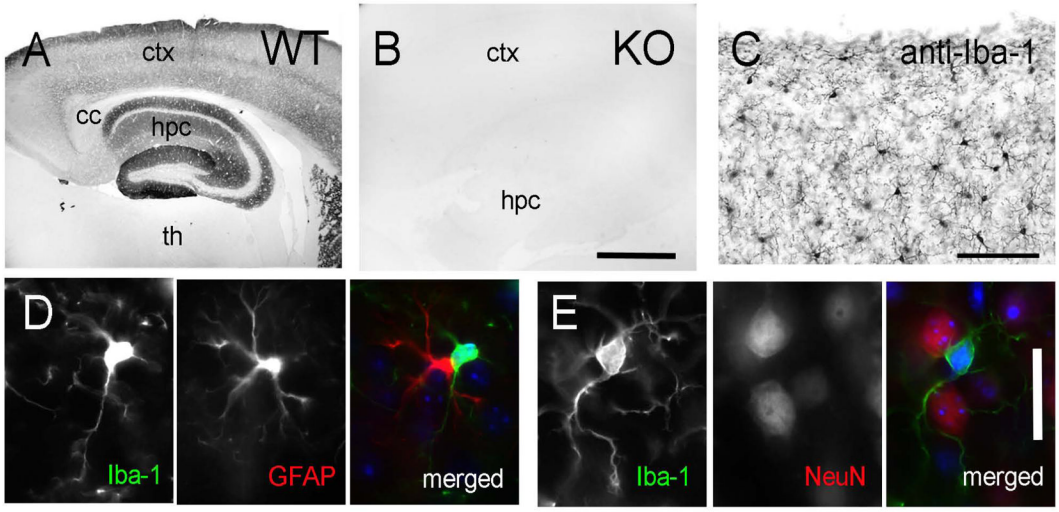

FIGURE 1. Immunocytochemical analysis of anti-ICAM-5 and anti-Iba-1 antibodies in mouse brain

(**A**) WT cortex shows ICAM-5 immunoreactivity in telencephalic structures (including hippocampus) but not in diencephalon (thalamus). (**B**) Anti-ICAM-5 immunohistochemistry in ICAM-5 KO cortex shows no immunoreactivity in telencephalic or diencephalic structures. (**C**) Anti-Iba-1 immunoreactivity in WT cortex shows specific labeling in microglial cell bodies and processes. (**D**) Immunofluorescent confirmation of anti-Iba-1 reactivity (first panel) with the astrocyte-specific marker, GFAP (second panel). The third panel is a merged image showing a lack of colocalization. Cell nuclei (DAPI counterstain) are denoted in blue. (**E**) Immunofluorescent confirmation of anti-Iba-1 immunoreactivity with the neuronal nuclei marker, NeuN. The third panel is a merged image showing a lack of colocalization. Cell nuclei (DAPI counterstain) are denoted in blue. Scale bar= (A–B) 1 mm; (C) 100 microns; (D,E) 25 microns. Abbreviations: ctx, cortex; hpc, hippocampus; th, thalamus; cc, corpus callosum.

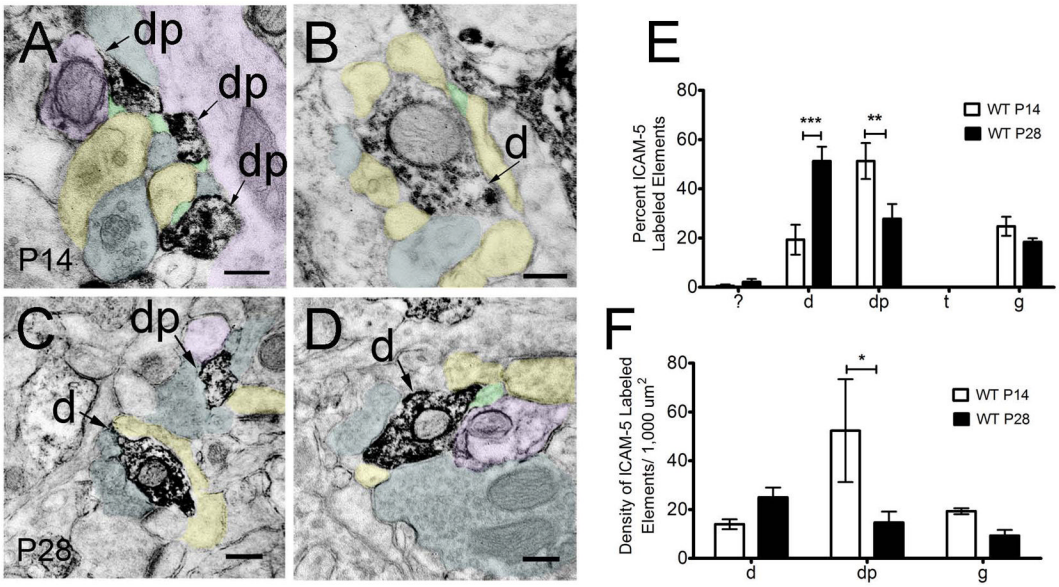

FIGURE 2. ICAM-5 Labeling in WT P14 and P28 mouse visual cortex

ICAM-5 labeled dendritic elements at P14 (**A–B**) and P28 (**C–D**). (**E**) ICAM-5 is found predominantly in dendritic protrusions during early visual development (P14) and in dendritic shafts during later development (P28). (**F**) At P14, the density of immunoreactive ICAM-5 dendritic protrusion is higher than at P28. *= $p<0.05$, ***= $p<0.001$; n=3 animals; 1,000 um^2 of neuropil analyzed for each animal. Labeling index= axon terminals (blue), dendrites (purple), dendritic protrusions (yellow), glia (green). Scale bars= 200 nm. Abbreviations: ?, unknown; d, dendrite; dp, dendritic protrusions; t, terminal; g, glia.

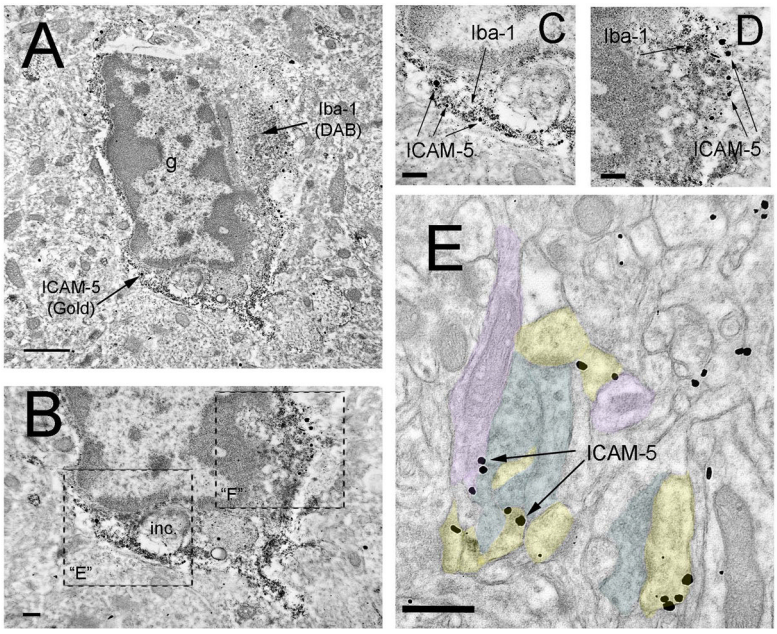

FIGURE 3. EM analysis of pre-embedding anti-Iba-1 and anti-ICAM-5 reactivity in P28 mouse visual cortex

(**A**) Low-magnification image of a characteristic microglial cell body (note condensed chromatin in the cell soma, vacuoles and other types of cytoplasmic inclusions) with anti-Iba-1 (visualized with a DAB precipitate) distributed throughout the cytoplasm. Anti-ICAM-5 (visualized with nanogold particles) is found primarily along the microglial plasma membrane. It should be noted that the surrounding elements of neuropil are devoid of non-specific immunogold staining (**B)** Larger magnification image of region in A showing a characteristic microglial inclusion (inc). (**C–D**) Magnified view of regions in B showing Iba-1 immunoreactivity in the microglial cytoplasm with ICAM-5 immunogold particles along the plasma membrane. (**E**) ICAM-5 immunogold reactivity in P28 mouse visual cortex. Arrows point to immunogold particles localized to dendritic membranes. Labeling index= axon terminals (blue), dendrites (purple), dendritic protrusions (yellow). Scale bars= (A) 1 mm; (B–D) 200 nm; (E) 500 nm. Abbreviations: inc= inclusion.

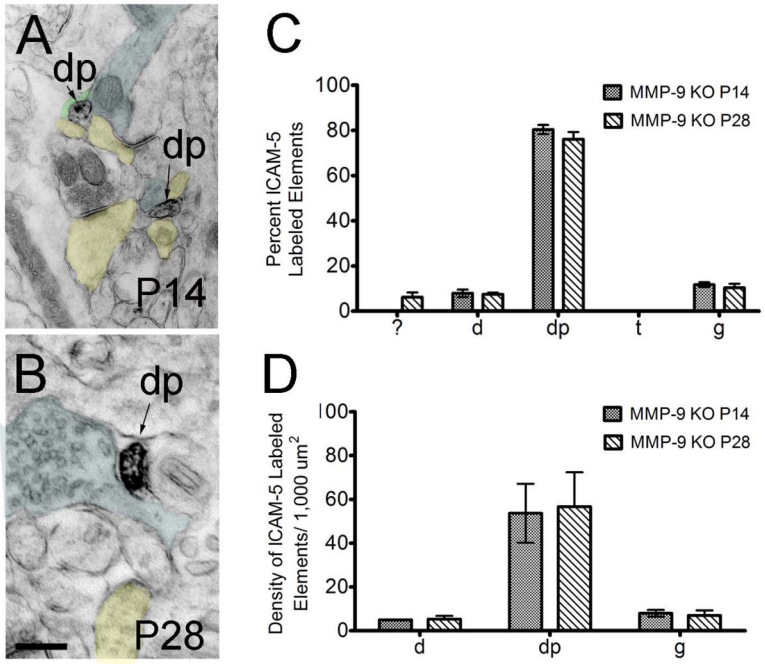

FIGURE 4. EM analysis of pre-embedding anti-ICAM-5 immunoperoxidase reactivity in P14 and P28 MMP-9 KO mouse visual cortex

(**A–B**) ICAM-5 labeled dendritic protrusions at P14 and P28. (**C**) The percent of ICAM-5 labeled elements in MMP-9 KO mice at P14 and P28 showed no significant differences in distribution across age. Immunoreactivity was found predominantly in dendritic protrusions at both ages. (**D**) A high density of immunoreactive dendritic protrusions was observed at P14 and P28. Labeling index= axon terminals (blue), dendritic protrusions (yellow), glia (green). Scale bar= 200 nm. Abbreviations: ?, unknown; d, dendrite; dp, dendritic protrusions; t, terminal; g, glia.

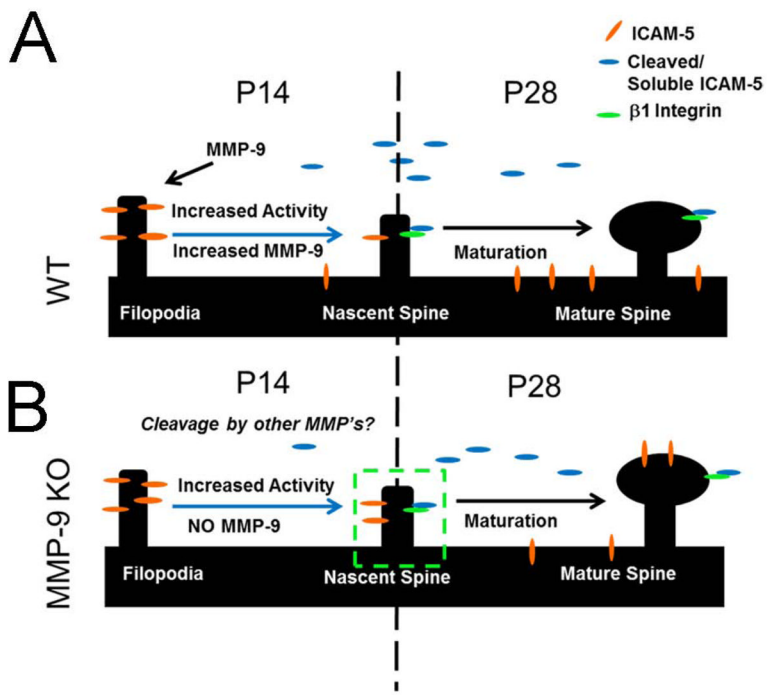

FIGURE 5. Localization of ICAM-5 is compromised in the absence of MMP-9

(**A**) ICAM-5 cleavage by MMP-9 regulates dendritic spine maturation. ICAM-5 is expressed in immature dendritic protrusions during early development (A, left side). Cleavage by MMP-9 results in the loss of ICAM-5 from putative spines, an increase in ICAM-5 in dendritic shafts and a resultant shift to a mature phenotype (A, right side). **(B)** In the absence of MMP-9 (KO), ICAM-5 is expressed initially in immature dendritic protrusions (B, bottom panel left side), and is retained in these structures as development proceeds (B, bottom panel, 'nascent spine'). Interestingly, we further found ICAM-5 retention in maturing dendritic protrusions by P28 (B, bottom panel, right side). This suggests a more complex relationship between ICAM-5 localization and synaptic maturation than previously envisioned. A possibility is that maturation effects may be mediated by soluble portions of ICAM-5 feeding back onto integrins in the dendritic spine.

Table 1

Primary Antibodies used.

Antigen	Immunogen	Manufacturer	Characterization Reference	Dilution Used
ICAM-5 cp	Intercellular adhesion molecule 5; Polyclonal antibody; Antiserum produced in rabbit, corresponding to the peptide sequence: AEGGAETPGT AESPADGEVF AIQLTSS which pertains to the last 17 amino acids in the C-terminus of mouse telencephalon.	Gift from Dr. Yoshihara; Brain Science Institute/Institute of Physical and Chemical Research (Wako City, Japan)	Yoshihara et. al., *Neuron*, **12**(3), 541 (1994).	1:500
Iba-1	Ionized calcium binding adaptor molecule 1; polyclonal antibody; synthetic peptide corresponding to the Iba-1 C-terminus, N′-PTGPPAKKAISELP-C′.	Wako Chemicals USA, Inc. (Richmond, VA), Catalog # 019-19741	Imai et. al., *Biochem. Biophys. Res. Commun.*, **224**, 855 (1996). *Journal of Comparative Neurology* anitbody database **ID # AB-2298770**.	1:1,000
GFAP	Glial fibrillary acidic protein; mouse monoclonal antibody reacts with the 50 kDA intermediate filament protein. Specifically, the epitope is localized on the C-Terminal Cys II fragment.	Sigma (St. Louis, MS), Catalog # C9205	Debus et. al., *Differentiation*, **25**, 193 (1983). *Journal of Comparative Neurology* antibody database **ID # 476889**	1:1,000
NeuN	Neuronal Nuclei; produced from purified cell nuclei from mouse brain. It recognizes fours bands between 45 and 75 kDa.	EMD Millipore Corp (Billerica, MA), Catalog # MAB377	Mullen et. al., *Development*, **116**, 201 (1992). *Journal of Comparative Neurology antibody database **ID # 94966***	1:500

Table 2

Quantitative Two-Way ANOVA analysis of ICAM-5 immuno-labeling in WT and MMP-9 KO Mice

WT P14 vs. MMP-9 KO P14	**WT P14**	**KO P14**	**t**	**P-value**
dendrite	19.33	7.967	1.647	NS
dendritic protrusions	51.27	76.93	3.718	p<0.05
MMP-9 KO P14 vs. WT P28	**KO P14**	**WT P28**	**t**	**P-value**
dendrite	7.967	51.26	6.272	P<0.001
dendritic protrusions	76.93	27.84	7.112	P<0.0001
WT P14 vs. WT P28	**WT P14**	**WT P28**	**t**	**P-value**
dendrite	19.33	51.26	4.625	P<0.01
dendritic protrusions	51.27	27.84	3.394	P<0.05
MMP-9 KO P14 vs. MMP-9 KO P28	**KO P14**	**KO P28**	**t**	**P-value**
dendrite	7.967	7.456	0.0739	NS
dendritic protrusions	76.93	76.05	0.1277	NS
WTP 14 vs. MMP-9 KO P28	**WT P14**	**KO P28**	**t**	**P-value**
dendrite	19.33	7.456	1.721	NS
dendritic protrusions	51.27	76.05	3.59	P<0.05
WT P28 vs. MMP-9 KO P28	**WT P28**	**KO P28**	**t**	**P-value**
dendrite	51.26	7.456	6.346	P<0.001
dendritic protrusions	27.84	76.05	6.985	P<0.0001

J Comp Neurol. Author manuscript; available in PMC 2015 February 15.